THE JOURNAL OF PHYSICAL CHEMISTRY B

Article

pubs.acs.org/JPCB

A Model Potential for Acetonitrile: from Small Clusters to Liquid

M. Albertí,*[,†] A. Amat,[‡] F. De Angelis,[‡] and F. Pirani[§]

[†]IQTCUB, Departament de Química Física, Universitat de Barcelona, Barcelona, Spain

[‡]Computational Laboratory for Hybrid/Organic Photovoltaics (CLHYO), Istituto CNR di Scienze e Tecnologie Molecolari, Perugia, Italy

[§]Dipartimento di Chimica, Università di Perugia, Perugia, Italy

Supporting Information

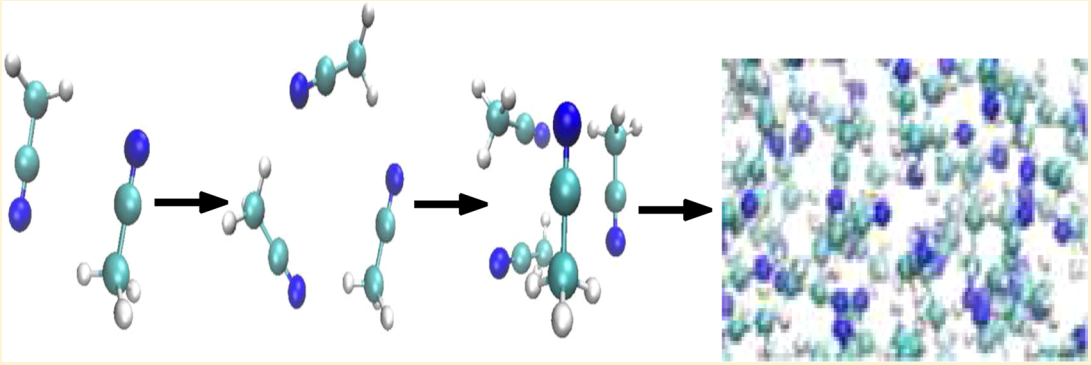

ABSTRACT: A portable model potential, representing the intermolecular interaction of acetonitrile with itself and with ions, is proposed. Such model, formulated as a combination of a few effective components, given in terms of the polarizability and dipole moment values of the molecular partners, is here adopted as a building block of the force field of acetonitrile clusters in molecular dynamics simulations. Its reliability is tested by comparing the predicted features for both small ionic and neutral clusters containing acetonitrile with ab initio results and experimental information. Its application to molecular dynamics simulations of liquid acetonitrile and of the solvated Li^+, Na^+, K^+, and I^-, performed at several values of the temperature, discloses an ample and interesting phenomenology, described in an internally consistent way. Such model will be useful to assess the effect of intermolecular interactions on the dynamics of acetonitrile processes occurring in various environments of applied relevance, with emphasis on the dye-sensitized solar cell framework.

1. INTRODUCTION

Acetonitrile (AN) is a polar aprotic liquid, able to solvate hydrophobic, hydrophilic, organic, and inorganic species.[1] In particular, AN is widely used as a solvent in the pharmaceutical industry in both manufacturing and analytical settings[2−4] and, due to its sufficient dispersive (hydrophobic) properties, is also employed to elute substances in chromatography.[5,6] A lot of AN comes as a byproduct of acrylonitrile in the industry of resins and plastics. AN can be used as a starting material to synthesize or analyze vitamins, cortisone, carbonate drugs, and some amino acids,[7] for spinning fibers,[8] for casting and molding of plastic materials,[9] and in lithium batteries.[10,11] Due to the unusually high value of its dipole moment, AN has attracted the attention of many scientists and it has been widely investigated from both theoretical[12−20] and experimental[21−25] viewpoint. AN is also used as a solvent for liquid electrolyte in dye-sensitized solar cells (DSCs).[26] Among the solar cells, DSCs have attracted great interest in the last years due to their moderate production cost and environmental impact when compared to the conventional Si p-n junction solar cells.[27−29] Moreover, these devices are flexible and color-transparent and can work under diffuse light conditions, characteristics that make them suitable in architecture and design. In DSCs, a dye sensitizer absorbs the solar radiation and transfers the photoexcited electron to a wide band gap semiconductor electrode, consisting of a mesoporous oxide layer composed of nanometer-sized particles, typically TiO_2. The electron then reaches a conducting glass and the cathode generating current. The system is regenerated by a redox couple that usually consists of iodide/triiodide in a solution of AN. Since the oxidized dye is regenerated thanks to the presence of the liquid electrolyte, understanding the interactions between the dye, the electrolyte, and the solvent is crucial to establish a solid ground useful to investigate DSCs regeneration mechanism and the dynamics of this process.[26,30,31]

Molecular dynamics (MD) simulations can be a useful tool to complement ab initio calculations and experimental results. Clearly, the reliability of the simulations largely depends on the accuracy of the force field used in MD, especially when considering the

Received: March 22, 2013
Revised: May 16, 2013

   dx.doi.org/10.1021/jp402827y | J. Phys. Chem. B XXXX, XXX, XXX−XXX

weakness of the individual interactions of AN with the dye, the electrolyte, and the semiconductor, which makes it difficult to assess the role of each interacting component. Recently, some of us have developed a potential model applied to investigate several systems, neutral (see, for instance, refs 32−34) and ionic (see, for instance, refs 35−37), at increasing complexity. The model predictions have been successfully compared with both accurate experiments and accurate ab initio calculations.[38−41] The main advantages of the model potential are its ability to describe properly both the most and the less stable configurations of the interacting complexes and its flexibility to investigate systems in different environments without changing the value of the most relevant potential parameters.[42] As a matter of fact, the behavior of both small water clusters and liquid water were investigated using the same values of the parameters that define the range and strength of the potential and varying only a parameter controlling its shape.[43]

In the present paper, we are interested in studying the acetonitrile interactions (small clusters and liquid) following the same methodology used previously for water interaction.[43] The aim of this study is to investigate in detail the features of the CH_3CN-CH_3CN, CH_3CN-Li^+, CH_3CN-Na^+, CH_3CN-K^+, and CH_3CN-I^- interactions in order to build and calibrate a suitable model to define the role of AN in the dye−electrolyte coupling which is key to the DSCs functioning.

Most of the results have been obtained by using MD methods. However, the interactions of acetonitrile with Li^+, Na^+, K^+, and I^- have also been analyzed from a static point of view, determining some relevant structural and energetic properties. The paper is organized as follows: the basic aspects of the model potential and the computational methodology are described in section 2, while statically predicted relevant properties of ion−CH_3CN are reported in section 3. MD results for both small clusters and acetonitrile are shown in section 4, and the concluding remarks are summarized in section 5.

2. COMPUTATIONAL METHODOLOGY

The ion−CH_3CN and CH_3CN-CH_3CN intermolecular interactions have been formulated by assuming the separability of electrostatic, V_{el}, and nonelectrostatic, V_{nel}, contributions. V_{nel} (see for instance ref 44) is calculated by considering the interaction centers placed on different groups of the molecule (atoms, bonds, etc.) with an assigned value of the polarizability.

The CH_3CN molecule is treated as a rigid body, where three interaction centers, localized on the CH_3, C and N groups (labeled hereafter as CM, C, and N), have been considered. Thus, the ion−CH_3CN intermolecular potential energy, V_{ion-CH_3CN}, is decomposed in ion−CM, ion−C, and ion−N interactions and it is described as

$$V_{ion-CH_3CN} = V_{ion-CM} + V_{ion-C} + V_{ion-N} + \sum_{i=1}^{6} \frac{q_i q_{ion}}{r_{i,ion}} \quad (1)$$

The first three terms represent the nonelectrostatic contribution ($V_{nel} = V_{ion-CM} + V_{ion-C} + V_{ion-N}$), while the last one, involving the six point charges placed on the atoms of CH_3CN, q_i, the ion charge, q_{ion}, and the distances between q_i and q_{ion}, defined by $r_{i,ion}$, accounts for the electrostatic one.

Similarly, the CH_3CN-CH_3CN intermolecular potential energy is given as

$$V_{CH_3CN-CH_3CN} = V_{(CM)_1-(CM)_2} + V_{(C)_1-(C)_2} + V_{(N)_1-(N)_2} + V_{(CM)_1-(C)_2} + V_{(CM)_1-(N)_2} + V_{(CM)_2-(C)_1} + V_{(CM)_2-(N)_1} + V_{(C)_2-(N)_1} + V_{(C)_1-(N)_2} + \sum_{i=1}^{6}\sum_{j=i}^{6} \frac{q_i q_j}{r_{i,j}} \quad (2)$$

Each nonelectrostatic term in eqs 1 and 2, depending on the balancing of a repulsive and an attractive component, is represented by an improved Lennard-Jones function (ILJ),[38,44] expressed as

$$V_{ILJ} = \varepsilon \left[\frac{m}{\beta + 4.0\left(\frac{r}{r_0}\right)^2 - m} \left(\frac{r_0}{r}\right)^{\beta + 4.0(r/r_0)^2} - \frac{\beta + 4.0\left(\frac{r}{r_0}\right)^2}{\beta + 4.0\left(\frac{r}{r_0}\right)^2 - m} \left(\frac{r_0}{r}\right)^m \right] \quad (3)$$

The relevant parameters ε (the well depth) and r_0 (the equilibrium distance) are determined from the effective values of the polarizability assigned to any pair of centers involved in the interaction.[45] The values of the polarizability assigned to the CM, C, and N centers, equal to 2.21, 1.0, and 1.1 Å^3, respectively, are compatible with the molecular polarizability of CH_3CN (α_{CH_3CN} = 4.31 Å^3). This partition of the CH_3CN polarizability compares well with other partitions found in the literature.[46−48] For the ions, we have considered the same values of the polarizability that in our previous studies (α_{Li^+} = 0.03 Å^3, α_{Na^+} = 0.18 Å^3, α_{K^+} = 0.85 Å^3, α_{I^-} = 7.53 Å^3).[39,40] The advantages of the ILJ function, which thanks to the additional shape parameter β with respect the LJ one removes most of the inadequacies of the LJ function at both short and long-range, have been discussed in detail before.[38,44]

Since the presence of the anion/cation significantly modifies the charge distribution accounting for the dipole moment of the single molecule of CH_3CN,[48] static calculations of the ion−CH_3CN properties have been performed by considering the electronic charges, and therefore the dipole moment, as adjustable parameters (in our model, the relevant parameters of the ILJ function, ε and r_0 are not adjustable). Then, for a given system, the optimized value of the dipole moment has been compared with results from DFT calculations using the B3LYP functional[49−51] and the 6-311++g** basis set.

In the absence of the ion and/or increasing the number of CH_3CN molecules in the system, the influence of the intermolecular electric field on the dipole moment of each monomer tends to vanish. This fact, together with the possibility of simulating AN solutions, suggests the adoption of only one CH_3CN charge distribution, independently of the ion. Therefore, we have used the charges and the dipole moment computed for the monomer to study the $(CH_3CN)_n$ (n = 2, 3, and 4) and ion−$(CH_3CN)_{36}$ small aggregates, the liquid AN, and the ion−liquid AN systems. However, due to the different characteristics of the small aggregates in comparison with the liquid AN and the ion−liquid AN systems, charge distributions in vacuo and in solvent have been calculated. The charge distribution to be used in eqs 1 and 2 has been computed using the Gaussian 09 package[52] by means of the MP2 method[53,54] and the 6-311++g** basis set in

dx.doi.org/10.1021/jp402827y | J. Phys. Chem. B XXXX, XXX, XXX−XXX

vacuo and in solvent by means of a polarizable continuum model CPCM.[55−57]

The EPS charge distribution obtained in vacuo has been used in MD simulations performed for the $(CH_3CN)_n$ (n = 2, 3, and 4) and ion−$(CH_3CN)_{36}$ systems in the gas phase considering a NVE ensemble of particles. On the contrary, the charge distribution optimized considering the solvent effects has been used to investigate both liquid AN and the solvated Li^+, Na^+, K^+, and I^- ions. For these larger systems (acetonitrile and solvated ions), NVE simulations have been only performed to thermalize the system at 230 K temperature. Once thermalized, the behavior of the systems, at higher temperatures and at 1 bar of pressure, has been characterized by using an isothermal−isobaric NpT ensemble, where the considered cell can freely expand or contract. In the NpT simulations, temperature and pressure are controlled using the Nosé−Hoover method,[58] and by applying the Berendsen algorithm,[59] respectively. The equilibration of the systems to achieve the desired values of T and p has been performed for 0.3 ns and the corresponding results have been excluded of the statistics carried out at the end of the simulation. Simulations along 10 ns (excluding equilibration) have been performed to investigate small clusters and AN. In both cases, a time step of 0.001 ps has been used. As usual, for the more complex molecular aggregates the electrostatic energy has been calculated by applying the Ewald sum[60] and in all simulations the CH_3CN has been kept rigid. The DL_POLY[61] program, where the subroutines of the potential and its derivatives have been implemented, has been used to carry out all MD calculations.

The potential parameters used to define the ILJ functions and the values of μ_{CH_3CN} considered are given in Table 1. The same values of β used to investigate the M^+−H_2O (M = Li, Na, K)[62] have been adopted here.

Table 1. ε (Well Depth), r_0 (Equilibrium Distance), β, and m Parameters Used to Define the Li^+−CH_3CN, Na^+−CH_3CN, K^+−CH_3CN, I^-−CH_3CN, and CH_3CN−CH_3CN Nonelectrostatic Interaction Contributions. Values of the CH_3CN Dipole Moment (See Text), μ_{CH_3CN}, Are Also Given

interaction partners	ε/meV	r_0/Å	β	m
Li^+−CM	267.41	2.571	4.5	4
Li^+−C	147.39	2.449	4.5	4
Li^+−N	157.65	2.466	4.5	4
μ_{CH_3CN} = 6.56 D				
Na^+−CM	176.55	2.901	6.0	4
Na^+−C	94.54	2.789	6.0	4
Na^+−N	101.47	2.805	6.0	4
μ_{CH_3CN} = 5.79 D				
K^+−CM	124.38	3.311	7.0	4
K^+−C	64.70	3.211	7.0	4
K^+−N	69.79	3.225	7.0	4
μ_{CH_3CN} = 5.40 D				
I^-−CM	73.72	4.262	7.0	4
I^-−C	34.96	4.202	7.0	4
I^-−N	38.17	4.211	7.0	4
μ_{CH_3CN} = 3.86 D				
CM−CM	10.268	4.122	8.5	6
CM−C	5.491	4.022	8.5	6
CM−N	5.935	4.035	8.5	6
C−C	3.003	3.910	8.5	6
C−N	3.231	3.926	8.5	6
N−N	3.483	3.941	8.5	6
μ_{CH_3CN} = 3.86 D				

3. ION−CH_3CN STATIC PROPERTIES

The potential energy surfaces (PESs) of Li^+−CH_3CN, Na^+−CH_3CN, K^+−CH_3CN, and I^-−CH_3CN have been computed by using the potential parameters reported in Table 1. The minimum potential energy and the geometry of all the investigated ion−molecule systems at its equilibrium are also predicted, and the corresponding values are compared with results from the literature. As it has been indicated above, the nonelectrostatic contributions have been represented by the ILJ function, while the electrostatic ones have been derived by applying the Coulomb law to pairs of point charges placed on different partners and compatible with the value of the CH_3CN dipole moment. The electrostatic charge of the cations and the anion favors approaches by the side of the nitrogen atom and by the side of the methyl group, respectively. As a matter of fact, in the minimum equilibrium structure the cations are placed close to the nitrogen atom of CH_3CN, while I^- is placed close to the methyl group of the molecule. In both cases, the ions lie along the CCN axis. This means that, in agreement with ab initio calculations,[63] the large dipole of the molecule is aligned along the electric field direction of the ions and that the ion−π interactions via the CN triple bond do not contribute to the stabilization of the ion−CH_3CN systems. As it has been indicated before,[42] the β parameter (see eq 3) adds flexibility to the ILJ function in comparison with the LJ one. As a matter of fact, its value can be used to take into account, indirectly, charge-transfer effects.[41,43] However, for the investigated cation−CH_3CN systems, a reasonable diminution of the value of β is insufficient to obtain good results of the interaction energy when the dipole moment of the isolated (gas phase) CH_3CN monomer (3.86 D) is used. This can be explained by the capabilities of the different interaction partners to polarize the CH_3CN molecule. Nguyen et al.[48] calculate an increase of μ_{CH_3CN} of about a 50% for the CH_3CN dimer and of about a 40%, and a 30% for CH_3CN in presence of Na^+ and I^-, respectively, while they observe a diminution of μ_{CH_3CN} when the size of the Na^+−$(CH_3CN)_m$ and I^-−$(CH_3CN)_m$ clusters increases. To take into account this phenomenon, in a previous study,[62] the increase of the dipole moment of water with respect to that of the isolated monomer was successfully used to investigate the M^+−H_2O (M = Li, Na, K) interactions. This study showed that Li^+, being the cation with the lowest polarizability (lowest size), leads to the highest increase of the dipole moment since it generates the highest electric field. The same strategy has been used in the present investigation to describe the M^+−CH_3CN interaction since also in this case, the interacting cations having a lower polarizability, α, than that of acetonitrile (μ_{CH_3CN} = 4.31 Å^3), they create strong electric fields and CH_3CN is highly polarized, specially in the case of Li^+. Using different charge distributions, we found out that, adopting the ones compatible with μ_{CH_3CN} values of 6.56, 5.79, and 5.40 D for the Li^+−(CH_3CN), Na^+−(CH_3CN), and K^+−(CH_3CN), respectively, a good agreement with ab initio calculations is obtained. In Table 2, the energy V_{min} of such ion−CH_3CN equilibrium structures and some relevant equilibrium distances are reported and compared to available data.[48,64−66] For the sake of consistency, the dipole moments of the CH_3CN fragments in the Li^+−(CH_3CN), Na^+−(CH_3CN), and K^+−(CH_3CN) clusters have been computed with B3LYP,

dx.doi.org/10.1021/jp402827y | J. Phys. Chem. B XXXX, XXX, XXX−XXX

Table 2. Ion−CH_3CN Minimum Potential Energy, V_{min}, and the Corresponding Nonelectrostatic, V_{nel}, and Electrostatic, V_{el}, Contributions. Distances $r_{cation-N}$ and $r_{anion-CM}$ Are Also Given[a]

cation−CH_3CN	V_{min}/meV	V_{nel}/meV	V_{el}/meV	r_{ion-N}/Å
present work				
Li^+-CH_3CN	−1841	−56	−1785	2.001
Na^+-CH_3CN	−1323	−47	−1276	2.338
K^+-CH_3CN	−1003	−37	−966	2.708
Li^+-CH_3CN	−1917,[64] −1814[65]			1.909,[64] 1.906,[65]
Na^+-CH_3CN	−1392,[64] −1331,[48] −1295[65]			2.283,[64] 2.310,[48] 2.293[65]
K^+-CH_3CN	−1097,[66] −1004[66]			2.759,[66] 2.759[66]
ion−CH_3CN	V_{min}/meV	V_{nel}/meV	V_{el}/meV	r_{ion-CM}/Å
present work				
I^-CH_3CN	−528	−66	−462	3.793
I^-CH_3CN[48]	−499			3.700

[a]The carbon atom of the methyl group is represented by CM.

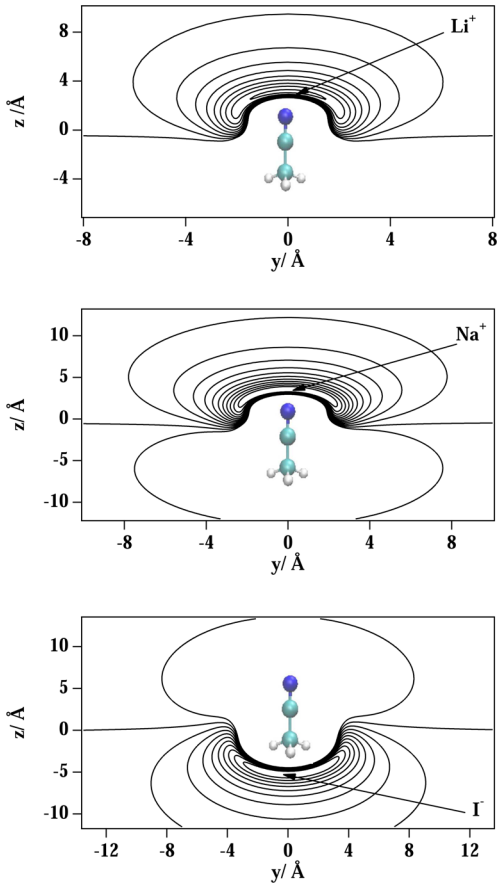

Figure 1. Li^+-CH_3CN (top panel), Na^+-CH_3CN (middle panel), and I^-CH_3CN (lower panel) potential energy surfaces. The lowest energy contours correspond to −1800 meV (top panel), −1200 meV (middle panel), and −500 meV (lower panel). Consecutive contours are equispaced by 200 meV (top panel), 150 meV (middle panel), and 75 meV (lower panel).

obtaining values of 6.24, 5.79, and 5.11 D, respectively, in line with the values obtained in the calibration of the ILJ calculations. Moreover, I^- being a strongly polarizable ion with a large size, for the $I^-(CH_3CN)$ system we obtained the best results without increasing the value of the dipole moment of the isolated monomer.

Finally, as it can be seen from Table 2, independently of the ion charge, the interaction is predominantly governed by electrostatic interaction.

All PESs show two well-differentiated regions, which are associated with approaches of cations by the side of N and by the side of the methyl group. For approaches of Li^+, Na^+, or K^+ to CH_3CN by the side of the N atom, pointing the NC−CM axis, the PES is very attractive while is repulsive from the other side. On the contrary, the PES for I^-CH_3CN is repulsive and attractive for approaches of I^- by the side of the N atom and the methyl group, respectively. These differences can be observed in Figure 1, where the PESs for Li^+-CH_3CN, Na^+-CH_3CN, and I^-CH_3CN are represented in the top, middle, and lower panels of the figure, respectively. As it can be seen by comparing top and middle panels of the figure, the potential energy surface is more attractive by the side of the CN group and more repulsive by the side of the methyl group, for the lightest cation.

4. MOLECULAR DYNAMICS

The potential parameters ε, r_0, and β given in Table 1 have been used to describe the nonelectrostatic energy contribution of the investigated systems, both in gas and in liquid phase. On the contrary, different charge distributions have been used to calculate the electrostatic energy contribution. While the $(CH_3CN)_{2-4}$ clusters and the ion−$(CH_3CN)_{36}$ systems have been investigated in the gas phase using the electrostatic potential fitting (ESP) charges computed in vacuo by MP2/6-311++g**, the charges computed at the same level of calculation but including solvent effects have been used to study the acetonitrile and the ion−acetonitrile systems in liquid phase. The values of the point charges are given as

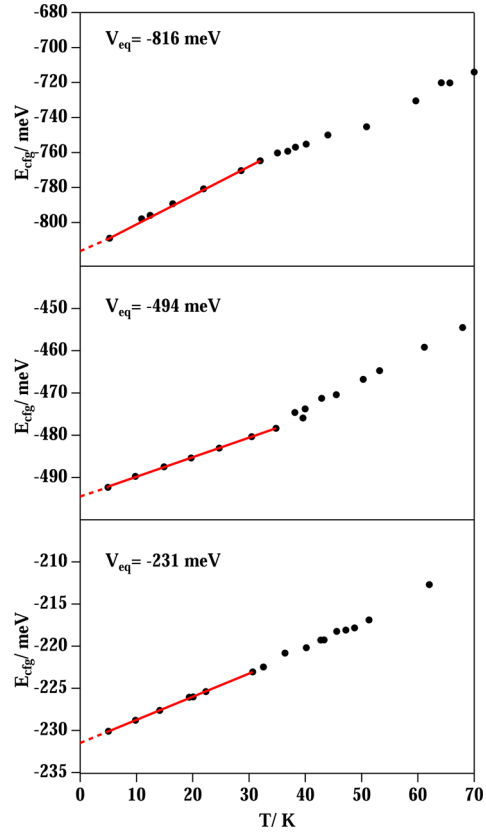

Figure 2. Mean potential energy, E_{cfg}, as a function of the temperature derived from MD simulations for $(CH_3CN)_2$ (lower panel), $(CH_3CN)_3$ (medium panel), and $(CH_3CN)_4$ (top panel).

dx.doi.org/10.1021/jp402827y | J. Phys. Chem. B XXXX, XXX, XXX−XXX

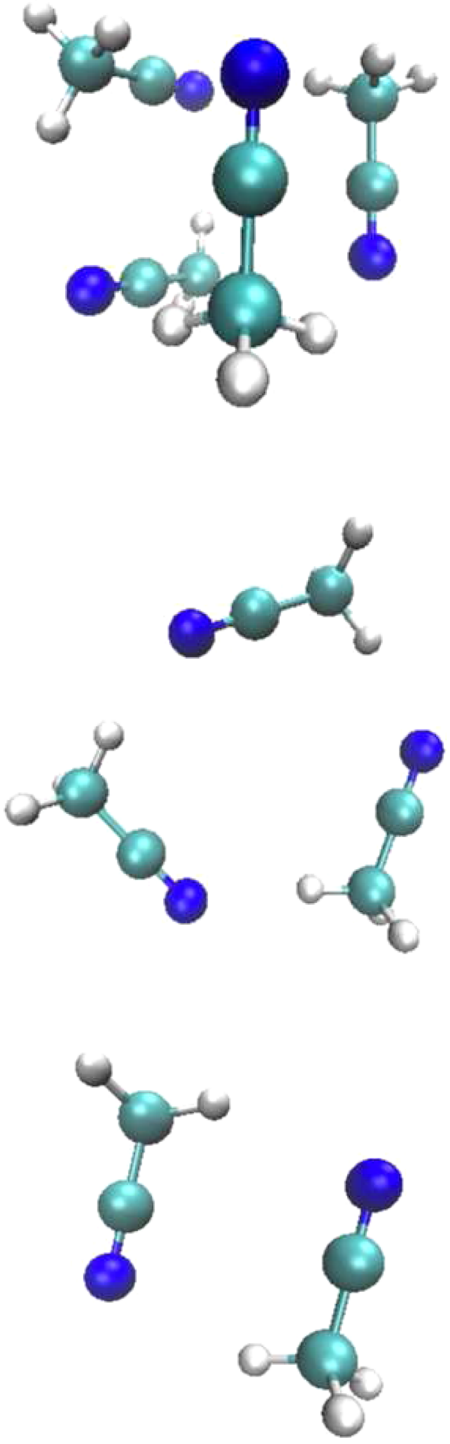

Figure 3. Equilibrium-like structures obtained by means of MD simulations at 15 K: configuration associated with the lower potential energy attained along the trajectory for the dimer (lower panel), trimer (medium panel), and tetramer (top panel).

Supporting Information. As it has been indicated before, both the $(CH_3CN)_{2-4}$ and the ion$-(CH_3CN)_{36}$ systems in the gas phase have been investigated from NVE simulations, while NpT simulations have been carried out to analyze both liquid acetonitrile and acetonitrile solvated ions in the liquid phase. MD simulations, independently of the considered ensemble, have been performed at increasing values of T. At each new temperature, the initial configuration was the last one of the previous simulation.

4.1. $(CH_3CN)_{2-4}$ Aggregates. To make an estimation of the $(CH_3CN)_{2-4}$ potential energy at equilibrium, simulations at several low values of T have been performed. Then, the mean values of the potential energy calculated along the trajectory, represented by the average configuration energies, E_{cfg}, have been extrapolated at $T = 0$. Rigorously, the characteristics of the global minima, as V_{min}, should be established by means of global optimization studies.[67,68] However, at low temperatures E_{cfg} varies linearly with T, and an estimation of the equilibrium energy (V_{eq}) can be obtained by extrapolating the values of E_{cfg} obtained at several temperatures at $T = 0$, as documented for small clusters containing N-methylacetamide.[33] The variation of the E_{cfg} values with T and the corresponding extrapolation to $T = 0$ are reported in Figure 2 for the acetonitrile dimer (lower panel), trimer (medium panel), and tetramer (top panel).

The estimated values of the equilibrium energy, indicated in the figure, and the geometries obtained are in agreement with results from HF, DFT, and MP2 calculations of the $(CH_3CN)_{2-4}$ clusters[16] and with DFT calculations on the $(CH_3CN)_{2-4}$ ones.[20] Moreover, to assess the accuracy of the MP2 and DFT data found in the literature for the $(CH_3CN)_{2-4}$ cluster, we have performed coupled-cluster CCSD(T) calculations[69−71] on the monomer and the dimer. Using the counterpoise correction[72,73] for the basis set superposition error (BSSE) in the intermolecular interaction, we compute an interaction energy for the dimer of 223 meV. Therefore, both the DFT[20] and MP2[16] interaction energies found in the literature and the results of the present work using the molecular dynamics are in good agreement with the CCSD(T) benchmark calculations. On the other hand, previous studies[20] concluded that the geometry of the isolated CH_3CN is almost unchanged by the presence of other molecules, thus justifying the optimization of larger CH_3CN clusters by freezing the monomer geometry in our MD simulations. The same previous theoretical investigation[20] indicates also that both HF and DFT underestimate the interaction energy between CH_3CN molecules when compared with ab initio correlated methods,[20] due to their failure in describing energies when noticeable dispersion effects are present.[74,75] The nonnegligible dispersion effects in AN interactions are manifested in the application of the symmetry-adapted perturbation theory (SAPT)[76] to the AN dimer ab initio calculations.[77]

Table 3. Interaction Energy at Equilibrium, in meV, for the $(CH_3CN)_n$ Clusters

			present work	
	MP2/6-31+G*[a] [16]	PW91/aug-cc-pVTZ[20]	CCSD(T)	pot. model
2	−211 (−252)	−227	−223	−231
3	−427 (−472)	−497		−494
4	−	−723		−816

[a]Numbers in parentheses are obtained with 6-311++G(2d,2p) basis set at the optimized 6-31+G* geometry.

Table 4. Intermolecular Distances and Angles of AN Dimers: $R_{C\cdots C}$, $R_{N\cdots H}$, $\theta_{N-C\cdots C}$, and $\theta_{CM-H\cdots N}$

	[a]MP2/6-31+G*[16]	PW91/aug-cc-pVDZ[20]	present
$R_{C\cdots C}$/Å	3.368	3.457	3.490
$R_{N\cdots H}$/Å	2.568	2.585	2.601
$\theta_{N-C\cdots C}$/deg	79.1	−	83.2
$\theta_{CM-H\cdots N}$/deg	132.9	138.3	139.3

[a]Numbers in parentheses are obtained with 6-311++G(2d,2p) basis set at the optimized 6-31+G* geometry.

dx.doi.org/10.1021/jp402827y | J. Phys. Chem. B XXXX, XXX, XXX−XXX

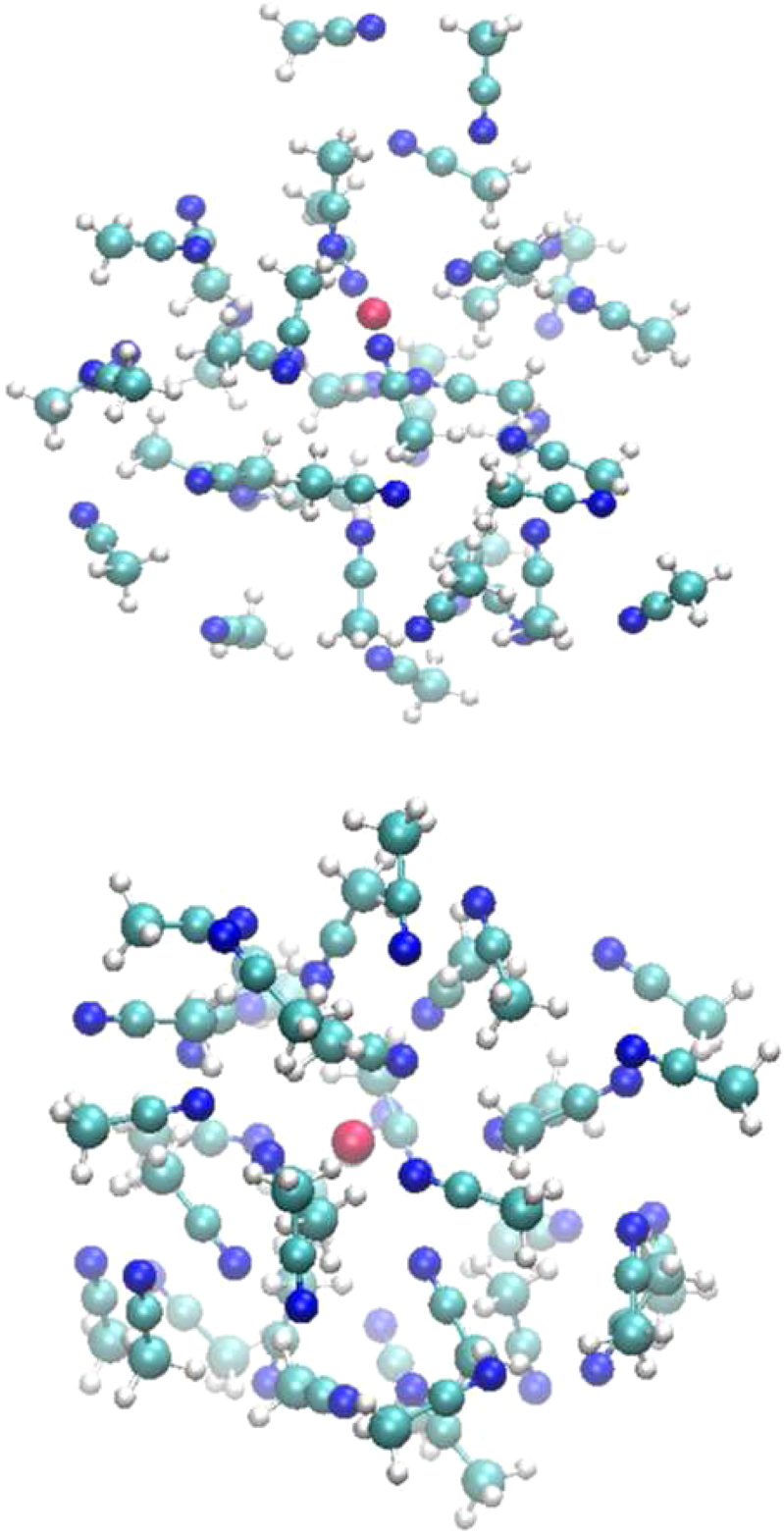

Figure 4. Representative structures of the $Li^+-(CH_3CN)_{36}$ (upper panel) and $I^-(CH_3CN)_{36}$ (lower panel) aggregates obtained at 275 K.

In agreement with previous studies,[16,20] our model predicts an antiparallel isomer and a cyclic structure as the more stable ones for dimer and trimer, respectively, the most stable structure for tetramer being the one with alternated pairs of molecules (see Figure 3).

In Table 3 the obtained equilibrium interaction energies are compared with the best results for the global minima obtained applying DFT and ab initio methodologies.

For simplicity, in the table all interaction energies, independently of the used methodology, are quoted as equilibrium energy. The higher differences are obtained for the tetramer, for which only DFT calculations have been found. However, Siebers et al.,[18] by combining an intramolecular force field[78] and a semiempirical intermolecular potential,[79] which is able to reproduce most of the features of the measured spectra, confirm a general

dx.doi.org/10.1021/jp402827y | J. Phys. Chem. B XXXX, XXX, XXX−XXX

tendency of CH_3CN clusters to grow in blocks of antiparallel dimers and compute a tetramer interaction energy of −858 meV in good agreement with our predictions. Further $(CH_3CN)_2$ and $(CH_3CN)_3$ calculations[79] are also in good agreement with our results, as well as the mean values of the distances and angles calculated from the configuration associated with the lowest value of the potential energy for the dimer (see Table 4).

The results obtained allow us to conclude that our potential model, as it has been observed in other systems, even being complex,[80] or including additional interaction effects,[37] is able to predict not only reliable values for the interaction energies but also the structural characteristics of the clusters. In addition, such models provide also the full potential energy surface in a proper analytical form.

4.2. Ion−$(CH_3CN)_{36}$ Aggregates. Representative structures for the $Li^+-(CH_3CN)_{36}$ and $I^-(CH_3CN)_{36}$ aggregates, obtained from MD simulations, are shown in the upper and lower panel of Figure 4, respectively.

From the upper panel of the figure it can be seen that, in the first solvation shell, the CH_3CN molecules are oriented with the N atom pointing toward Li^+ while the first solvation shell in the $I^-(CH_3CN)_{36}$ aggregates (bottom panel) seems to be less compact. This behavior can be attributed to the interaction of the I^- ion with the three H atoms of the methyl group and to the flat potential energy zone when I^- moves around CH_3. These differences can be also observed when comparing the radial distribution functions (RDFs) (cation···N) with the RDF(I^-···CM). The first ones show two well-defined peaks (whose positions are given in Table 5) indicating an inner solvation structure in agreement with results found for $Na^+-(CH_3CN)_{36}$.[48]

Table 5. Positions of the First and Second Peak, R_1 and R_2, Respectively, on the RDFs of Ion−$(CH_3CN)_{36}$ Aggregates Obtained at 273 K

system	$R_1{}^a$/Å	$R_2{}^a$/Å
$Li^+-(CH_3CN)_{36}$	2.225	5.875
$Na^+-(CH_3CN)_{36}$	2.425	6.075
$K^+-(CH_3CN)_{36}$	2.825	6.525
$I^-(CH_3CN)_{36}$	5.275	8.975

$^aR_1$ and R_2 means the distance from the cation to N atom for the cation−$(CH_3CN)_{36}$ aggregates and the distance from I^- to the C atom of the methyl group for $I^-(CH_3CN)_{36}$, respectively.

At the same conditions, the RDF(I^-···CM) peaks are much broader, indicating a lower organization of the solvation shells for the $I^-(CH_3CN)_{36}$ aggregates, which is probably due to both the combined interaction of I^- with the three H atoms and the flat potential energy surface when I^- approaches the CH_3CN molecules by the side of the methyl group. These results are corroborated by the coordination numbers along the cation/anion distance to N/CM, which show a defined plateau evidencing the presence of well-defined cells for the cation−$(CH_3CN)_{36}$ aggregates, not present for $I^-(CH_3CN)_{36}$ (see Figure 5).

Coordination numbers equal to 6 are found when acetonitrile solvates Li^+ and Na^+ and equal to 7 when K^+ is the solvated ion. Due to the absence of a definite plateau it is difficult to establish a coordination number for the solvated I^-. Our predictions can be compared with the results of Nguyen et al.,[48] which indicate that the first solvation shell for Na^+ contains 5.9 acetonitrile molecules. The same authors indicate that the first solvation shell for I^- contains approximately 8 molecules, while our results seem to indicate an aproximate coordination number around 9−10 molecules.

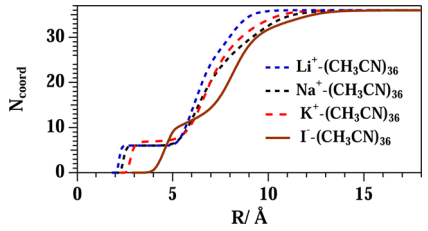

Figure 5. Coordination number, $N_{coord}(R)$, for the ion−$(CH_3CN)_{36}$ aggregates (R means both the cation−N and the anion−CM distances). $N_{coord}(R)$ has been normalized to converge to the total number of solvent molecules at large distances.

4.3. Liquid Acetonitrile. For the representation of liquid AN an ensemble of 343 CH_3CN molecules placed in a cubic box of 31 Å of side has been thermalized at 230 K considering a NVE ensemble. Then, liquid AN has been investigated by means of NpT simulations in the 230−345 K range and at the pressure of 1 bar. An increase of T, as expected, originates a decrease of the density (d) and an increase of the mean diffusion coefficient values (D) (see Figure 6).

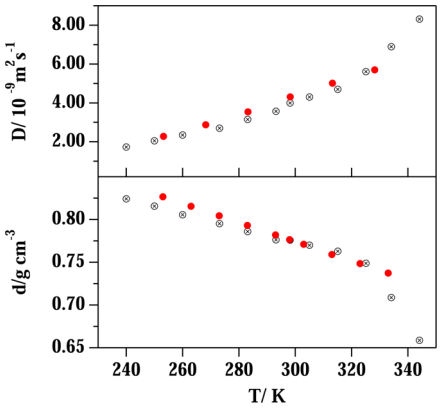

Figure 6. Mean diffusion coeficients (upper panel) and density (lower panel) for the pure acetonitrile obtained by means MD simulations using a NpT ensemble at several temperatures (N = 343, p = 1 bar). Red circles correspond to experimental results.[81,82]

As it can be seen, from 230 to 345 K, MD calculations predict a smooth increase/decrease of D/d with T, while, at higher temperatures, sharper variations of D and d are observed. This fact is indicative of temperatures close to the boiling point ($T_{boiling}$ = 354.7 K). The obtained results are compared with experimental data represented as red circles in Figure 6. In particular, the predicted density values are compared with the Dortmund data (liquid 3)[81] and as it can be seen in the lower panel of the figure, the agreement is very good. On the top panel of the same figure, the obtained values of the diffusion coefficient are compared with the experimental values of Hurle and Woolf obtained at the pressure of 1 bar.[82] Also in this case, the agreement of the simulation data with experimental results is excellent.

Previous studies indicate that AN is a scarcely structured liquid, exhibiting order only at short distances.[83] This means that two neighboring molecules tend to lie in an antiparallel arrangement but different pairs do not follow any order. Bearing in mind this molecular organization, in which the dipoles of two molecules are oppositely aligned, liquid acetonitrile can be viewed as an ensemble of "inert" molecular pairs. Insights on the structure of liquid acetonitrile have been deduced from the

dx.doi.org/10.1021/jp402827y | J. Phys. Chem. B XXXX, XXX, XXX−XXX

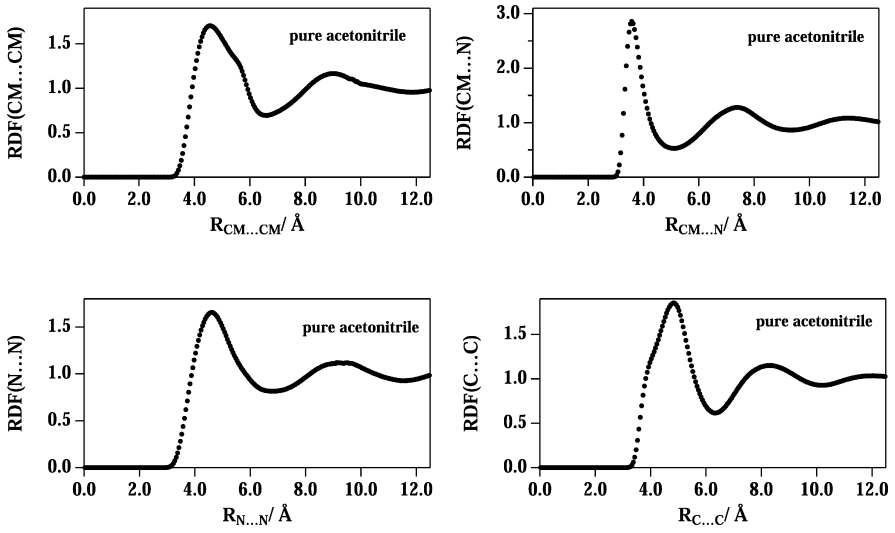

Figure 7. Pure acetonitrile radial distribution functions derived from MD simulations using a *NpT* ensemble of 343 molecules of CH_3CN at 273 K and 1 bar of pressure. Methyl carbon−methyl carbon (CM···CM, upper left-hand side panel), nitrogen−nitrogen (N···N, lower left-hand side panel), methyl carbon−nitrogen (CM···N, upper right-hand side panel), and nitrile carbon−nitrile carbon (C···C, lower right-hand side panel).

Table 6. Configuration Energy, E_{cfg}, for Pure Acetonitrile and for the Solvated Ions at the Temperature of 273 K and 1 bar of Pressure

system	AN	solvated Li^+	solvated Na^+	solvated K^+	solvated I^-
E_{cfg}/eV	−148.80 ± 0.03	−156.97 ± 0.06	−155.95 ± 0.06	−155.02 ± 0.07	−153.10 ± 0.04

obtained RDFs. In Figure 7 the RDFs between methyl groups (CM···CM), methyl carbon and N atom (CM···N), N atoms (N···N), and nitrile carbon atoms (C···C) are shown in the upper left, upper right, lower left, and lower right panels, respectively.

The RDFs, which are very similar to those previously published,[17,65,79,83,84] have been derived from MD simulations at T = 273 K and p = 1 bar. The RDF(CM···CM) shows a first peak at $R_{CM\cdots CM}$ = 4.575 Å with a shoulder at larger distances, in agreement with previously published acetonitrile interaction potentials.[17] The RDF(CM···N), showing the sharpest maximum ($R_{CM\cdots N} \approx$ 3.4 Å) among all RDFs, reflects the strong interaction between the methyl group and the N atom. The RDF(N···N) is broader, due to the fact of the antiparallel CH_3CN disordered pairs. The maximum peak at $R_{N\cdots N} \approx$ 4.6 Å is slightly shorter than the $R_{N\cdots N}$ equilibrium distance on the dimer. The RDF(C···C), in qualitative agreement with results derived from ab initio[83,84] and empirical[79,85] pair potentials, shows a broad peak at $R_{C\cdots C} \approx$ 4.8 Å including a shoulder at shorter distances ($R_{C\cdots C} \approx$ 3.8 Å). On the other hand, X-ray diffraction experimental results[24] show a broad peak at 3−5 Å in the RDF of pure acetonitrile, which was explained well only when both antiparallel and parallel dipole−dipole orientations were assumed for the first- and second-neighbor molecules. In our study, the broad peak appears at a distance from the methyl groups which is about 0.3 Å larger than that derived from X-ray experiments. However, the RDF(CM−CM) peak is very similar and it is also due to the parallel and antiparallel arrangements. Moreover, as it can be observed in the upper right-hand side panel of Figure 7, the first peak of the RDF(CM−N) is narrower and it appears at a shorter value of the distance than the RDF(CM−CM) one. This should indicate that the antiparallel orientation of the dipoles is preferred between the first neighbor, in agreement with the combined neutron and X-ray experiments of Bertagnolli and Zeidler,[86] which indicate that the antiparallel orientation of the dipoles is preferred between the first neighbors.

4.4. Ion−Liquid Acetonitrile Systems. The solvated acetonitrile ions have been investigated by placing one ion in the center of the box containing 343 acetonitrile molecules. However, previously to the study of the ion solvation by means of MD simulations, the effect of using different acetonitrile optimized charge distributions has been properly assessed. The calculations, performed before for the ion−$(CH_3CN)_{36}$ aggregates using charges optimized in vacuum, have been repeated using the charges computed with MP2/6-311++g** including the solvent effects. For the new equilibrium energy of the simplest ion−CH_3CN systems, only small differences have been detected, again the interaction energy of Li^+−CH_3CN being the highest one. Estimated values of V_{eq} equal to −1645, −1303, −1033, and −534 meV for Li^+−CH_3CN, Na^+−CH_3CN, K^+−CH_3CN, and I^-−CH_3CN, respectively, have been obtained with the inclusion of solvent effects to the charge distribution. Moreover, it has been observed that the increase of the charge on the central C atom originates a very flat I^-−CH_3CN potential energy surface around the methyl group and in this zone the potential energy is almost independent of the orientation when I^- approaches CH_3CN by the side of CH_3. Thus, while the equilibrium structures for the cation−CH_3CN systems are very similar to those obtained before, that for I^-−CH_3CN is slightly different, the C−CM···I^- angle being equal to 145° instead of 180°. However, due to the flatness of the potential energy surface around CH_3, we think that the distortion of the equilibrium geometry does not affect the dynamics of the system when I^- is surrounded by several molecules of acetonitrile.

As it has been indicated above, MD simulations of the ion-solvated systems have been performed by adding the ion in the center of the cell box of AN molecules thermalized at a given temperature. By comparing solvated ions with both the ion−$(CH_3CN)_{36}$ aggregates and pure AN, it has been observed that the structure of the first solvation shell remains almost unaffected when the number of CH_3CN molecules increases from 36 to 343.

dx.doi.org/10.1021/jp402827y | J. Phys. Chem. B XXXX, XXX, XXX−XXX

The ions, as it was observed for the smaller aggregates, interact strongly with the CH_3CN molecules placed on the first solvation shell, originating only small differences on the configuration energy (E_{cfg}) of pure AN respect to that of the solvated ions (see Table 6).

Taking into account the values of the interaction energy for the ion−CH_3CN systems given in Table 2 and those given in Table 6, it seems that the presence of the ions slightly modifies the structure of AN beyond the first solvation shell. Some representative RDFs are shown in Figure 8 where the RDF(Li^+···N) and the RDF(I^-···CM) are represented in the upper and lower panels, respectively.

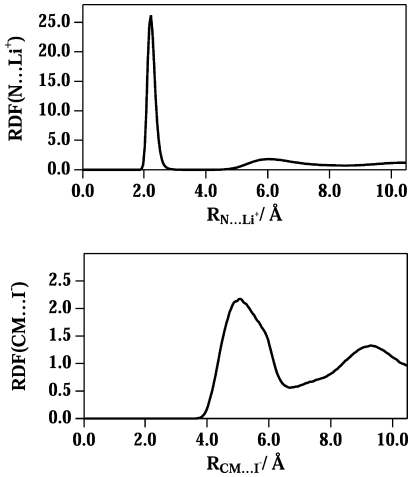

Figure 8. Radial distribution functions derived from MD simulations using a *NpT* ensemble of 343 molecules of CH_3CN solvating Li^+ and I^- at 273 K of temperature and 1 bar of pressure: Li^-···N (top) and I^-···CM (bottom).

As observed for the Li^+−$(CH_3CN)_{36}$ and I^-−$(CH_3CN)_{36}$ aggregates (see Table 5), the form of the first solvation peak is different, indicating that the first solvation shell around Li^+ is much more structured than that around I^-. The position and form of the first peak for the solvated Li^+ are very similar to those obtained for the smaller aggregates. These similarities between the solvated ions and the ion−$(CH_3CN)_{36}$ aggregates have been also observed for the systems containing Na^+ and K^+. The RDFs (N···cation) show peaks at 2.225, 2.425, and 2.775 Å, for Li^+, Na^+, and K^+, respectively, which are nearly coincident with the results of Table 5. The RDF(I^-···CM) shown in the lower panel of Figure 8 also looks very similar to RDFs of the $I^-(CH_3CN)_{36}$ aggregates, with the first peak much broader than those observed for cation−$(CH_3CN)_{36}$ aggregates.

To have a clearer view on whether or not the AN structure is altered by the presence of ions, the RDFs data of Figure 7 are compared in Figure 9 with those for the solvated Li^+ and I^-. As it can be seen, the acetonitrile RDFs do not depend on the charge of the ion.

The addition of Li^+ or I^- to acetonitrile does not affect the RDF(CM···CM) and RDF(N···N) of pure acetonitrile, while some changes in the position of the first peak are observed in the RDF(CM···N) and RDF(C···C). These facts seem to indicate that the presence of the ions tends to reduce the CM···CM and the CM···N distances between the two acetonitrile molecules in the antiparallel pairs. As before, the results are independent of the cation and similar RDFs have been obtained when Li^+ is substituted by Na^+ and K+.

5. CONCLUDING REMARKS

Some small aggregates containing CH_3CN molecules, liquid acetonitrile, and the acetonitrile solvation of Li^+, Na^+, K^+, and I^- have been investigated by means of molecular dynamics simulations. The involved intermolecular interactions have been first modeled by decomposing them in electrostatic and nonelectrostatic contributions, the last ones being described by means of the ILJ function, whose relevant parameters have been derived from values of the polarizability assigned to the ions and to different groups on the CH_3CN molecule, compatible with the whole molecular polarizability. The same ILJ parameter values have been used to model the interactions, independently of the size of the aggregates. The presence of an ion creates a strong electric field in its vicinity and the CH_3CN molecule is highly polarized, inducing a modification of the molecular charge distributions that leads to an increase of the dipole moment of the CH_3CN monomer, which tends to a constant value when the number of CH_3CN molecules increases. This fact allows to

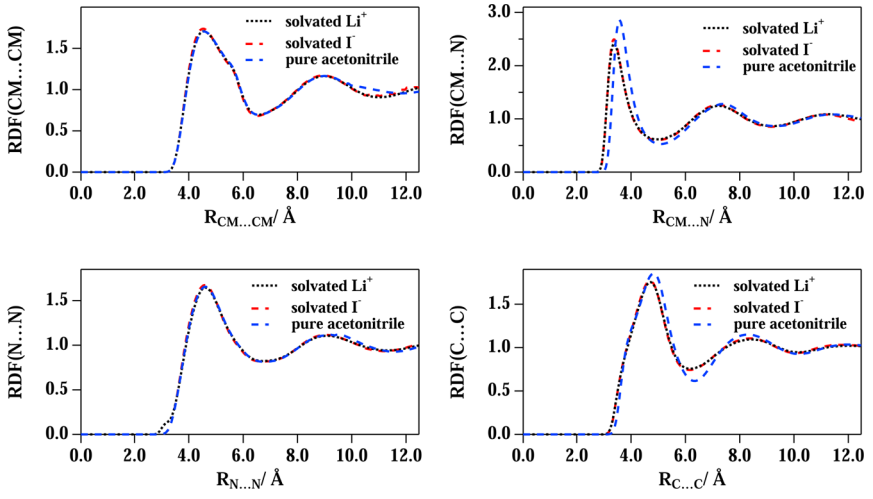

Figure 9. Radial distribution functions derived from MD simulations using a *NpT* ensemble of 343 molecules of CH_3CN solvating Li^+ and I^- at 273 K and 1 bar of pressure. Methyl carbon−methyl carbon (CM···CM, upper left-hand side panel), nitrogen−nitrogen (N···N, lower left-hand side panel), methyl carbon−nitrogen (CM···N, upper right-hand side panel), and nitrile carbon−nitrile carbon (C···C, lower right-hand side panel). RDFs for pure acetonitrile are included for comparison.

dx.doi.org/10.1021/jp402827y | J. Phys. Chem. B XXXX, XXX, XXX−XXX

investigate both the liquid acetonitrile and the solvated systems using the same value of μ_{CH_3CN}. The model predicts equilibrium geometry and energy values of the small aggregates in agreement with pevious results from ab initio calculations. The density and diffusion coefficients of the liquid AN agree with experimental information in the 230−345 K temperature range. Moreover, the obtained RDFs are similar to the predictions of other potential models. The cation−acetonitrile systems show more structured first solvation shells than that for the I^-−acetonitrile, which can be due both to the stronger cation−CH_3CN interaction in comparison with the I^-−CH_3CN one and to the fact that I^- simultaneously interacts with the three hydrogen atoms of the methyl group, while the cations interact with the N atom, originating a high directionality on the cation−CH_3CN interactions that favors the formation of high structured solvation shells. The obtained static and molecular dynamics results allow to conclude that the potential model is able to satisfactorily predict, in an internally consistent way, the main energy and geometry characteristics of the small clusters and to obtain a description of the liquid acetonitrile and of the solvated ions in agreement with results available in the literature. Furthermore, within the scheme approach it is possible to describe properly both more and less stable conformations of the examined systems.

The methodology that we have setup in this work will be applied in future studies to analyze the crucial interactions of iodine/triiodine and a prototype dye molecule in a liquid AN environment. These investigations will allow to get insight on the regeneration process of the oxidized dye in the framework of liquid-electrolyte DSCs.

■ ASSOCIATED CONTENT

Supporting Information

CH_3CN charge distributions are given. This material is available free of charge via the Internet at http://pubs.acs.org.

■ AUTHOR INFORMATION

Corresponding Author

*E-mail: m.alberti@ub.edu.

Notes

The authors declare no competing financial interest.

■ ACKNOWLEDGMENTS

M.A. acknowledges financial support from the Ministerios de Educación y Ciencia (Spain, Project CTQ2010-16709) and to the Comissionat per a Universitats i Recerca del DIUE (Generalitat de Catalunya, Project 2009-SGR 17). Also thanks are due to the SUR and the Departament d'Economia i Coneixement de la Generalitat de Catalunya (Project 2011 BE1-00063) and to the Centre de Serveis Científics i Acadèmics de Catalunya CESCA and Fundació Catalana per a la Recerca for the allocated supercomputing time. A.A. and F.D.A. thank FP7-NMP-2009 Project 246124 "SANS" for financial support. F.P. acknowledges financial support the Italian Ministry of University and Research (MIUR) for a PRIN Grant.

■ REFERENCES

(1) Sazonov, V. P.; Shaw, D. G. IUPAC-NIST Solubility Data Series. 78. Acetonitrile Binary Systems. *J. Phys. Chem. Ref. Data* **2002**, *31*, 989−1133.

(2) Schmidt, A. H. Validated HPLC Method for the Determination of Residues of Acetaminophen, Caffeine, and Codeine Phosphate on Swabs Collected from Pharmaceutical Manufacturing Equipment in Support of Cleaning Validation. *J. Liq. Chromatogr.* **2006**, *29*, 1663−1673.

(3) Kumar, N.; Sangeetha, D.; Balakrishna, P. Development and Validation of a UPLC Method for the Determination of Duloxetine Hydrochloride Residues on Pharmaceutical Manufacturing Equipment Surfaces. *Pharm. Methods* **2011**, *2*, 161−166.

(4) Wen, Z.-Q.; Li, G.; Ren, D. Detection of Trace Melamine in Raw Materials Used for Protein Pharmaceutical Manufacturing Using Surface-Enhanced Raman Spectroscopy (SERS) with Gold Nanoparticles. *Appl. Spectrosc.* **2011**, *65*, 514−521.

(5) Cunha, S. C.; Fernandes, J. O. Multipesticide Residue Analysis in Maize Combining Acetonitrile-Based Extraction with Dispersive Liquid-Liquid Microextraction Followed by Gas Chromatography Mass Spectrometry. *J. Chromatogr. A* **2011**, *1218*, 7748−7757.

(6) Salvia, M.-V.; Vulliet, E.; Wiest, L.; Baudot, R.; Cren-Olivé, C. Development of a Multi-Residue Method Using Acetonitrile-Based Extraction Followed by Liquid Chromatography Tandem Mass Spectrometry for the Analysis of Steroids and Veterinary and Human Drugs at Trace Levels in Soil. *J. Chromatogr. A* **2012**, *1245*, 122−133.

(7) Ono, N. *The Nitro Group in Organic Synthesis*; John Wiley and Sons, Inc.: New York, 2001.

(8) Wannatong, L.; Sirivat, A.; Supaphol, P. Effects of Solvents on Electrospun Polymeric Fibers: Preliminary Study on Polystyrene. *Polym. Int.* **2004**, *53*, 1851−1859.

(9) Edwards, T. L.; Harper, J. C.; Polsky, R.; Lopez, A. M.; Wheeler, D. R.; Allen, A. C.; Brozik, S. M. A Parallel Microfluidic Channel Fixture Fabricated Using Laser Ablated Plastic Laminates for Electrochemical and Chemiluminescent Biodetection of DNA. *Biomicrofluidics* **2011**, *5*, 044115−044129.

(10) Kim, J.; Lee, D.-J.; Jung, H.-G.; Sun, Y.-K.; Hassoun, J.; Scrosati, B. Lithium-Sulfur Batteries: An Advanced Lithium-Sulfur Battery. *Adv. Funct. Mater.* **2013**, *23*, 1076−1080.

(11) Fanga, S.; Zhanga, Z.; Jina, Y.; Yanga, L.; Hiranob, S.-I.; Tachibanac, K.; Katayamad, S. New Functionalized Ionic Liquids Based on Pyrrolidinium and Piperidinium Cations with Two Ether Groups as Electrolytes for Lithium Battery. *J. Power Sources* **2011**, *196*, 5637−5644.

(12) Cabaleiro-Lago, E. M.; Ríos, M. A. A Potential Function for Intermolecular Interaction in the Acetonitrile Dimer Constructed from ab Initio Data. *J. Phys. Chem. A* **1997**, *101*, 8327−8334.

(13) Cabaleiro-Lago, E. M.; Ríos, M. A. Intermolecular Potential for Acetonitrile Based on ab initio Calculations Intermolecular Potential for Acetonitrile based on ab initio Calculations. *Mol. Phys.* **1999**, *96*, 309−321.

(14) Richardi, J.; Fries, P. H.; Krienke, H. Influence of the Intermolecular Electrostatic Potential on Properties of Polar Polarizable Aprotic Solvents. *Mol. Phys.* **1999**, *96*, 1411−1422.

(15) Grabuleda, X.; Jaime, C.; Kollman, P. A. Molecular Dynamics Simulation Studies of Liquid Acetonitrile: New Six-Site Model. *J. Comput. Chem.* **2000**, *21*, 901−908.

(16) Cabaleiro-Lago, E. M.; Hermida-Ramón, J. M.; Peña-Gallego, A.; Martínez Núñez, E.; Fernández Ramos, A. Intermolecular Interactions and Cooperative Effects in Acetonitrile Clusters. An ab initio Molecular Orbital Study. *J. Mol. Struct. (Theochem)* **2000**, *498*, 21−28.

(17) Guàrdia, E.; Pinzón, R.; Casulleras, J.; Orozco, M.; Luque, F. J. Comparison of Different Three-site Interaction Potentials for Liquid Acetonitrile. *Mol. Simul.* **2001**, *26*, 287−306.

(18) Siebers, J. G.; Buck, U.; Beu, T. A. Calculation of Structures and Vibrational Spectra of Acetonitrile Clusters. *Chem. Phys.* **1998**, *239*, 549−560.

(19) Mountain, R. D. Shear Viscosity and Dielectric Constant of Liquid Acetonitrile. *J. Chem. Phys.* **1997**, *107*, 3921−3923.

(20) Mata, R. A.; Costa Cabral, B. J. Structural, Energetic, and Electronic Properties of $(CH_3CN)_{2-8}$ Clusters by Density Functional Theory. *J. Mol. Struct. (Theochem)* **2004**, *673*, 155−164.

(21) Ohba, T.; Ikawa, S. Far-Infrared Optical Constants of Liquid Acetonitrile at 238 to 343 K as Measured with a Synchrotron Radiation Source. *Mol. Phys.* **1991**, *73*, 985−997.

(22) Stolov, A. A.; Kamalova, D. I.; Borisover, M. D.; Solomonov, B. N. Hydrogen Bonds Formed by Methyl Groups of Acetonitrile: Infrared and Calorimetric Study. *Spectrochim. Acta A* **1994**, *50*, 145−150.

(23) Dessent, C. E. H.; Kim, J.; Johnson, M. A. Evidence for the High-Energy (Collinear) van der Waals Isomer of the Acetonitrile Dimer. *J. Phys. Chem.* **1996**, *100*, 12−14.
(24) Takamuku, T.; Tabata, M.; Yamaguchi, A.; Nishimoto, J.; Kumamoto, M.; Wakita, H.; Yamaguchi, T. Liquid Structure of Acetonitrile-Water Mixtures by X-ray Diffraction and Infrared Spectroscopy. *J. Phys. Chem. B* **1998**, *102*, 8880−8888.
(25) Ding, F.; Hu, Z.; Zhong, Q.; Manfred, K.; Gattass, R. R.; Brindza, M. R.; Fourkas, J. T.; Walker, R. A.; Weeks, J. D. Interfacial Organization of Acetonitrile: Simulation and Experiment. *J. Phys. Chem. C* **2010**, *114*, 17651−17659.
(26) Boschloo, G.; Hagfeldt, A. Characteristics of the Iodide/Triiodide Redox Mediator in Dye-Sensitized Solar Cells. *Acc. Chem. Res.* **2009**, *42*, 1819−1826.
(27) O'Regan, B.; Grätzel, M. A Low-Cost, High-Efficiency Solar Cell Based on Dye-Sensitized Colloidal TiO_2 Films. *Nature* **1991**, *353*, 737−740.
(28) Nazeeruddin, M. K.; De Angelis, F.; Fantacci, S.; Selloni, A.; Viscardi, G.; Liska, P.; Ito, S.; Takeru, B.; Grätzel, M. Combined Experimental and DFT-TDDFT Computational Study of Photoelectrochemical Cell Ruthenium Sensitizers. *J. Am. Chem. Soc.* **2005**, *127*, 16835−16847.
(29) Grätzel, M. Recent Advances in Sensitized Mesoscopic Solar Cells. *Acc. Chem. Res.* **2009**, *42*, 1788−1798.
(30) Schiffmann, F.; VandeVondele, J.; Hutter, J.; Urakawa, A.; Wirz, R.; Baiker, A. An Atomistic Picture of the Regeneration Process in Dye Sensitized Solar Cells. *Proc. Natl. Acad. Sci. U.S.A.* **2010**, *107*, 4830−4833.
(31) Schiffmann, F.; Hutter, J.; VandeVondele, J.; Atomistic Simulations of a Solid/Liquid Interface: a Combined Force Field and First Principles Approach to the Structure and Dynamics of Acetonitrile Near an Anatase Surface *J. Phys.: Condens. Matter* **2008**, *20*, 064206 (1−8).
(32) Albertí, M. Rare Gas-Benzene-Rare Gas Interactions: Structural Properties and Dynamic Behavior. *J. Phys. Chem. A* **2010**, *114*, 2266−2274.
(33) Albertí, M.; Faginas Lago, N.; Laganà, A.; Pirani, F. A Portable Intermolecular Potential for Molecular Dynamics Studies of NMA-NMA and NMA-H_2O Aggregates. *Phys. Chem. Chem. Phys.* **2011**, *13*, 8422−8432.
(34) Cappelletti, D.; Candori, P.; Falcinelli, S.; Albertí, M.; Pirani, F. A molecular beam scattering investigation of methanol-noble gas complexes: Characterization of the Isotropic Potential and Insights into the Nature of the Interaction. *Chem. Phys. Lett.* **2012**, *545*, 14−20.
(35) Albertí, M.; Pacifici, L.; Laganà, A.; Aguilar, A. A Molecular Dynamics Study for the Isomerization of Ar Solvated $(Benzene)^2$-K^+ Heteroclusters. *Chem. Phys.* **2006**, *327*, 105−111.
(36) Albertí, M.; Aguilar, A.; Lucas, J. M.; Pirani, F. Static and Dynamic Properties of Anionic Intermolecular Aggregates: the I^--Benzene-Ar_n Case. *Theor. Chem. Acc.* **2009**, *123*, 21−27.
(37) Albertí, M.; Aguilar, A.; Pirani, F. Cation-π-Anion Interaction in Alkali Ion-Benzene-Halogen Ion Clusters. *J. Phys. Chem. A* **2009**, *113*, 14741−14748.
(38) Pirani, F.; Brizi, S.; Roncaratti, L. F.; Casavecchia, P.; Cappelletti, D.; Vecchiocattivi, F. Beyond the Lennard-Jones Model: a Simple and Accurate Potential Function Probed by High Resolution Scattering Data Useful for Molecular Dynamics Simulations. *Phys. Chem. Chem. Phys.* **2008**, *10*, 5489−5640.
(39) Albertí, M.; Aguilar, A.; Lucas, J. M.; Pirani, F.; Cappelletti, D.; Coletti, C.; Re, N. Atom-Bond Pairwise Additive Representation for Cation-Benzene Potential Energy Surfaces: An ab Initio Validation Study. *J. Phys. Chem. A* **2006**, *110*, 9002−9010.
(40) Albertí, M.; Aguilar, A.; Lucas, J. M.; Pirani, F.; Coletti, C.; Re, N. Atom-Bond Pairwise Additive Representation for Halide-Benzene Potential Energy Surfaces: an Ab Initio Validation Study. *J. Phys. Chem. A* **2009**, *113*, 14606−14614.
(41) Albertí, M.; Aguilar, A.; Lucas, J. M.; Pirani, F. Competitive Role of CH_4-CH_4 and CH-π Interactions in C_6H_6-$(CH_4)_n$ Aggregates: The Transition from Dimer to Cluster Features. *J. Phys. Chem. A* **2012**, *116*, 5480−5490.
(42) Albertí, M.; Aguilar, A.; Lucas, J. M.; Pirani, F. A Generalized Formulation of Ion-π Electron Interactions: Role of the Non-electrostatic Component and Probe of the Potential Parameter Transferability. *J. Phys. Chem. A* **2010**, *114*, 11964−11970.
(43) Albertí, M.; Aguilar, A.; Bartolomei, M.; Cappelletti, D.; Laganà, A.; Lucas, J. M.; Pirani, F. A Study to Improve the van der Waals Component of the Interaction in Water Clusters *Phys. Scr.* **2008**, *78*, 058108 (1−7).
(44) Pirani, F.; Albertí, M.; Castro, A.; Moix, M.; Cappelletti, D. Atom-Bond Pairwise Additive Representation for Intermolecular Potential Energy Surfaces. *Chem. Phys. Lett.* **2004**, *394*, 37−44.
(45) Pirani, F.; Cappelletti, D.; Liuti, G. Range, Strength and Anisotropy of Intermolecular Forces in Atom-Molecule Systems: an Atom-Bond Pairwise Additivity Approach. *Chem. Phys. Lett.* **2001**, *350*, 286−296.
(46) Thole, B. T. Molecular Polarizabilities Calculated with a Modified Dipole Interaction. *Chem. Phys.* **1981**, *59*, 341−350.
(47) Miller, K. J. Additivity Methods in Molecular Polarizability. *J. Am. Chem. Soc.* **1990**, *112*, 8533−8542.
(48) Nguyen, T.-N.; Hughes, S. R.; Peslherbe, G. H. Microsolvation of the Sodium and Iodide Ions and Their Ion Pair in Acetonitrile Clusters: A Theoretical Study. *J. Phys. Chem. B* **2008**, *112*, 621−635.
(49) Becke, A. D. Density functional thermochemistry III. The role of exact exchange. *J. Chem. Phys.* **1993**, *98*, 5648−4652.
(50) Lee, C.; Yang, W.; Parr, R. G. Development of the Colle-Salvetti correlation-energy formula into a functional of the electron density. *Phys. Rev. B* **1998**, *37*, 785−789.
(51) Miehlich, B.; Savin, A.; Stoll, H.; Preuss, H. Results obtained with the correlation energy density functionals of Becke and Lee, Yang and Parr. *Chem. Phys. Lett.* **1989**, *157*, 200−206.
(52) Frisch, M. J.; Trucks, G. W.; Schlegel, H. B.; Scuseria, G. E.; Robb, M. A.; Cheeseman, J. R.; Scalmani, G.; Barone, V.; Mennucci, B. et al. *Gaussian 09, Revision A.1*; Gaussian, Inc.: Wallingford, CT, 2009.
(53) Head-Gordon Pople, J. A.; Frisch, J. MP2 Energy Evaluation by Direct Methods. *Chem. Phys. Lett.* **1998**, *153*, 503−506.
(54) Head-Gordon, M.; Head-Gordon, T. Analytic MP2 Frequencies without Fifth-Order Sstorage. Theory and Application to Bifurcated Hydrogen Bonds in the Water Hexamer. *Chem. Phys. Lett.* **1994**, *220*, 122−128.
(55) Cossi, M.; Rega, N.; Scalmani, G.; Barone, V. Energies, Structures, and Electronic Properties of Molecules in Solution with the C-PCM Solvation Model. *J. Comput. Chem.* **2003**, *24*, 669−681.
(56) Cossi, M.; Barone, V. Separation between Fast and Slow Polarizations in Continuum Solvation Models. *J. Phys. Chem. A* **2000**, *104*, 10614−10622.
(57) Cossi, M.; Barone, V. Time-Dependent Density Functional Theory for Molecules in Liquid Solutions. *J. Chem. Phys.* **2001**, *115*, 4708−4717.
(58) Nosé, S. A Molecular Dynamics Method for Simulations in the Canonical Ensemble. *Mol. Phys.* **1984**, *52*, 255−268.
(59) Berendsen, H. J. C.; Postma, J. P. M.; Vangunsteren, W. F.; Dinola, A.; Haak, J. R. Molecular Dynamics with Coupling to an External Bath. *J. Chem. Phys.* **1984**, *81*, 3684−3690.
(60) Ewald, P. P. Quantum Fields and Interactions of Massless Particles: the Continuous Spin Case. *Ann. Phys.* **1921**, *64*, 253−287.
(61) http://www.cse.scitech.ac.uk/ccg/software/DL−POLY/.
(62) Albertí, M.; Aguilar, A.; Cappelletti, D.; Laganà, A.; Pirani, F. On the Development of an Effective Model Potential To Describe Water Interaction in Neutral and Ionic Clusters. *Int. J. Mass Spectrom.* **2009**, *280*, 50−56.
(63) Vaden, T. D.; Lisy, J. M. Competing Non-covalent Interactions in Alkali Metal Ion-Acetonitrile-Water Clusters. *J. Phys. Chem. A* **2005**, *109*, 3880−3886.
(64) Cabaleiro-Lago, E. M.; Rios, M. A. Ab Initio Study of $M(CH_3CN)_n$ Clusters ($M=Li^+$, Na^+, Mg^{2+}) in the Gas Phase. *Chem. Phys.* **2000**, *254*, 11−23.

(65) Spångberg, D.; Hermansson, K. The Solvation of Li^+ and Na^+ in Acetonitrile from Ab Initio-Derived Many-Body Ion-Solvent Potentials. *Chem. Phys.* **2004**, *300*, 165−176.
(66) Islam, M. S.; Pethrick, R. A.; Pugh, D. Ab Initio Study of Potassium Ion Clusters of Methanol and Acetonitrile and a Systematic Comparison with Hydrated Clusters. *J. Phys. Chem. A* **1998**, *102*, 2201−2208.
(67) Schulz, F.; Hartke, B. Dodecahedral Clathrate Structures and Magic Numbers in Alkali Cation Microhydration Clusters. *ChemPhysChem* **2002**, *3*, 98−106.
(68) Llanio-Trujillo, J. L.; Marques, J. M. C.; Pereira, F. B. An Evolutionary Algorithm for the Global Optimization of Molecular Clusters: Application to Water, Benzene, and Benzene Cation. *J. Phys. Chem. A* **2011**, *115*, 2130−2138.
(69) Purvis, G. D., III; Bartlett, A. Full Coupled-Cluster Singles and Doubles Model - the Inclusion of Disconnected Triples. *J. Chem. Phys.* **1982**, *76*, 1910−1918.
(70) Scuseria, G. E.; Janssen, C. L.; Schaefer, H. F., III An Efficient Reformulation of the Closed-Shell Coupled Cluster Single and Double Excitation (CCSD) Equations. *J. Chem. Phys.* **1988**, *89*, 7382−7387.
(71) Pople, J. A.; Head-Gordon, M.; Raghavachari, K. Quadratic Configuration Interaction. A General Technique for Determining Electron Correlation Energies. *J. Chem. Phys.* **1987**, *87*, 5968−5975.
(72) Boys, S. F.; Bernardi, F. The Calculation of Small Molecular Interactions by the Differences of Separate Total Energies. Some Procedures with Reduced Errors. *Mol. Phys.* **1970**, *19*, 553−566.
(73) Simon, S.; Duran, M.; Dannenberg, J. J. How Does Basis Set Superposition Error Change the Potential Surfaces for Hydrogen-Bonded Dimers? *J. Chem. Phys.* **1996**, *105*, 11024−11031.
(74) Perdew, J. P.; Wang, Y. Accurate and Simple Analytic Representation of the Electron-Gas Correlation Energy. *Phys. Rev. B* **1992**, *45*, 13244−13249.
(75) Tsuzuki, S.; Lüthi, H. P. Interaction Energies of van der Waals and Hydrogen Bonded Systems Calculated Using Density Functional Theory: Assessing the PW91 Model. *J. Chem. Phys.* **2001**, *114*, 3949−3957.
(76) Jeziorski, B.; Moszynski, R.; Szalewicz, K. Perturbation Ttheory Approach to Intermolecular Potential Energy Surfaces of van der Waals Complexes. *Chem. Rev.* **1994**, 1887−1930.
(77) Bukowski, R.; Szalewicz, K.; Chabalowski, C. F. Ab Initio Interaction Potentials for Simulations of Dimethylnitramine Solutions in Supercritical Carbon Dioxide with Cosolvents. *J. Phys. Chem. A* **1999**, *103*, 7322−7340.
(78) Duncan, J. L.; McKean, D. C.; Tullini, F.; Nivellini, G. D.; Pérez Peña, J. Methyl cianide: Spectroscopic Studies of Isotopically Substituted Species, and the Harmonic Potential Function. *J. Mol. Spectrosc.* **1978**, *69*, 123−140.
(79) Böhm, H. J.; McDonald, I. R.; Madden, P. A. An Effective Pair Potential for Liquid Acetonitrile. *Mol. Phys.* **1983**, *49*, 347−360.
(80) Albertí, M.; Costantini, A.; Laganà, A.; Pirani, F. Are Micelles Needed to Form Methane Hydrates in Sodium Dodecyl Sulfate Solutions? *J. Phys. Chem. B* **2012**, *116*, 4220−4227.
(81) http://www.ddbst.com/en/EED/PCP/DEN−C3.php.
(82) Hurle, R. L.; Woolf, L. A. Self-Diffusion in Liquid Acetonitrile Under Pressure. *J. Chem. Soc., Faraday Trans. 1* **1982**, *78*, 2233−2238.
(83) Cabaleiro-Lago, E. M.; Ríos, M. A. An Intermolecular Potential Function for Na^+-Acetonitrile Obtained from Ab Initio Calculations.: Application to Liquid Simulations. *Chem. Phys.* **1998**, *236*, 235−242.
(84) Sum, A. K.; Sandler, S. I.; Bukowski, R.; Szalewicz, K. Prediction of the Phase Behavior of Acetonitrile and Methanol with Ab Initio Pair Potentials. I. Pure components. *J. Chem. Phys.* **2002**, *116*, 7627−7636.
(85) Jorgesen, W. L.; Briggs, J. M. Monte Carlo Simulations of Liquid Acetonitrile with a Three-Site Model. *Mol. Phys.* **1988**, *63*, 547−558.
(86) Bertagnolli, H.; Zeidler, M. D. Molecular Pair-Correlation Function of Liquid Acetonitrile from X-ray and Neutron Diffraction Studies. *Mol. Phys.* **1978**, *35*, 177−192.